Chemical Science

ROYAL SOCIETY OF CHEMISTRY

EDGE ARTICLE

View Article Online
View Journal | View Issue

Cite this: *Chem. Sci.*, 2020, **11**, 1342

All publication charges for this article have been paid for by the Royal Society of Chemistry

Received 4th December 2019
Accepted 17th December 2019

DOI: 10.1039/c9sc06150a

rsc.li/chemical-science

Switchable electrical conductivity in a three-dimensional metal–organic framework *via* reversible ligand n-doping†

Hanna C. Wentz,[a] Grigorii Skorupskii,[b] Ana B. Bonfim,[a] Jenna L. Mancuso,[c] Christopher H. Hendon,[c] Evan H. Oriel,[d] Graham T. Sazama[d] and Michael G. Campbell *[a]

Redox-active metal–organic frameworks (MOFs) are promising materials for a number of next-generation technologies, and recent work has shown that redox manipulation can dramatically enhance electrical conductivity in MOFs. However, ligand-based strategies for controlling conductivity remain underdeveloped, particularly those that make use of reversible redox processes. Here we report the first use of ligand n-doping to engender electrical conductivity in a porous 3D MOF, leading to tunable conductivity values that span over six orders of magnitude. Moreover, this work represents the first example of redox switching leading to reversible conductivity changes in a 3D MOF.

Introduction

Electrically conductive porous metal–organic frameworks (MOFs) have emerged as a fascinating class of materials with potential impact in a wide variety of applications, enabled by the development of chemical design strategies that overcome the longstanding problem of inherent insulating behavior in porous crystalline solids.[1] For example, the development of layered 2D MOFs with extended π–d conjugation has led to record-setting conductivity values while maintaining permanent porosity in some cases.[2] Engendering conductivity in 3D MOFs has been significantly more challenging, but recent work has shown that open-shell metal centers and/or organic ligands can be used to increase charge carrier density, coupled with either through-bond or through-space charge transport pathways.[1a,3] Guest@MOF strategies have also been developed to impart conductivity on otherwise insulating framework materials, by insertion of electroactive guest molecules or polymers into the MOF pores.[4]

One strategy, with the potential to be quite general, is to make use of redox-active components in the MOF.[5] Redox manipulation of a stable, insulating MOF can be used to increase electrical conductivity while maintaining structural integrity, and both chemical and electrochemical doping approaches can be envisioned. Examples of this strategy to date have been dominated by redox-active metal centers in the secondary building units (SBUs), and iron-based SBUs have shown particular promise.[6] For example, partial reduction of the Fe(III) centers to Fe(II) in the material $Fe_2(BDP)_3$ (BDP = 1,4-benzenedipyrazolate) results in electrical conductivity increases up to four orders of magnitude.[7] Similarly, partial aerobic oxidation of Fe(II) centers in $Fe_2(BDT)_3$ (BDT = 1,4-benzeneditetrazolate) leads to tunable conductivity values that span five orders of magnitude.[8] Analogous approaches that make use of ligand-based redox activity in 3D MOFs are less developed, and have focused primarily on materials with non-innocent semiquinone or dithiolene-type linkages.[9] Furthermore, there have been no examples of reversible redox processes that can be used to reversibly modulate conductivity in a 3D MOF, for either metal- or ligand-based approaches.

In this work, we show that n-doping of the redox-active naphthalene diimide (NDI) organic ligands in the microporous pyrazolate MOF ZnNDI (Fig. 1a) can produce a greater than one-million-fold enhancement in conductivity. The ligand-based reduction can be performed reversibly without altering the structure of the framework, and the extent of ligand reduction can be used to tune the material's conductivity over several orders of magnitude. To the best of our knowledge, this represents the first example of appreciable electrical conductivity in a 3D MOF as a result of reductive ligand doping. Furthermore, while redox switching has been used to control conductivity in 1D and 2D coordination polymers,[10] this is the first demonstration of reversible switching between two different stable redox states with dramatically different conductivity values for a 3D MOF.

[a]Department of Chemistry, Barnard College, New York, New York 10027, USA. E-mail: mcampbel@barnard.edu

[b]Department of Chemistry, Massachusetts Institute of Technology, Cambridge, Massachusetts 02139, USA

[c]Department of Chemistry and Biochemistry, University of Oregon, Eugene, Oregon 97403, USA

[d]Department of Chemistry, Lawrence University, Appleton, Wisconsin 54911, USA

† Electronic supplementary information (ESI) available: Experimental procedures, details of DFT calculations, and supplementary data figures. See DOI: 10.1039/c9sc06150a

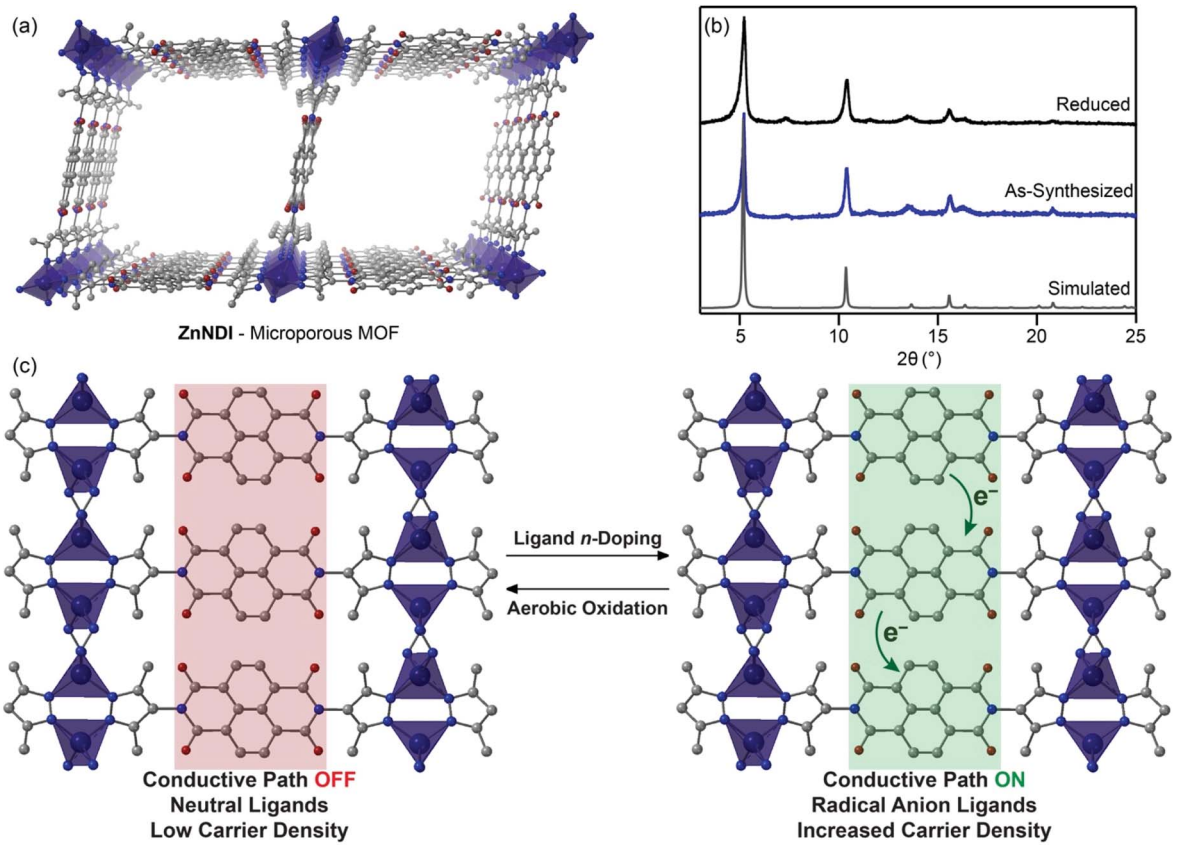

Fig. 1 (a) Structure of the microporous MOF ZnNDI; (b) PXRD data demonstrating that the MOF structure remains intact after ligand reduction; (c) the ordered stacks of NDI ligands undergo reversible reduction to their radical anion form, creating a through-space charge transport pathway *via* NDI hopping that results in increased electrical conductivity.

Redox activity of NDI-based ligands in MOFs has previously been used for applications such as electrochromic devices.[11] The NDI subunits of the ligands typically exhibit well-behaved electrochemistry, displaying reversible reduction processes to their $NDI^{\bullet -}$ radical anion and NDI^{2-} dianion states. In this work, we make use of the known fluoride-induced reduction of NDIs as a mild chemical doping strategy that can reversibly transform the neutral ligands in ZnNDI to their radical anion form;[12,13] while the specific mechanism of NDI reduction in the presence of fluoride is still a matter of debate in the literature, recent work suggests a complex solvent-mediated pathway.[14] The ordered stacks of $NDI^{\bullet -}$ ligands generated in this manner form a charge transport pathway that dramatically increases the framework's conductivity (Fig. 1c). Supramolecular organization has been shown to both promote and stabilize the formation of NDI radical anions,[15] and the rigid ordering provided by the crystalline MOF provides advantages compared to solution-phase approaches toward conductive stacks of NDI radicals.[16]

Results and discussion

ZnNDI was synthesized according to the reported procedure as a microcrystalline tan/yellow powder; PXRD analysis confirmed the expected structure (Fig. 1b).[17] Ligand reduction was carried out by soaking ZnNDI in DMF solutions of tetra-*n*-butylammonium fluoride (TBAF). In order to qualitatively evaluate the effect of soaking time on ligand reduction, we performed UV-vis measurements using thin films of ZnNDI grown on the surface of glass slides (Fig. 2). The pale films of as-

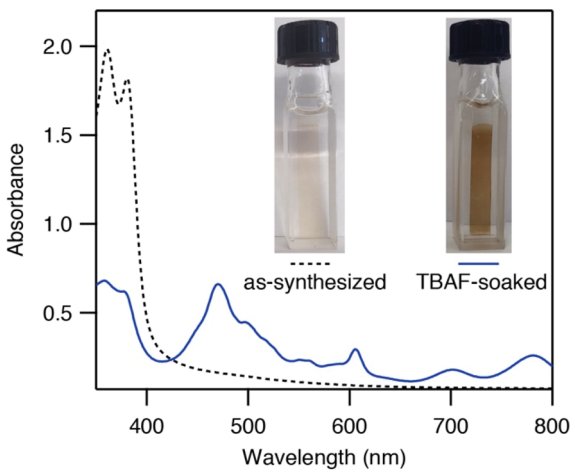

Fig. 2 UV-vis data of a ZnNDI thin film before and after soaking in a TBAF solution (60 mM in DMF, 14 hours), showing conversion of the neutral NDI ligands to their radical anion form; the inset shows optical images of the films.

synthesized ZnNDI display absorption maxima at 360 and 380 nm, assigned to $\pi \rightarrow \pi^*$ transitions in the neutral NDI ligands. Upon placing the film into a TBAF solution the color gradually darkens, accompanied by a decrease in intensity for the neutral NDI features and the appearance of new features throughout the visible region (λ_{max} = 471, 607, 701, 784 nm). These features are characteristic of $NDI^{\bullet -}$ radical anions,[18] and correspond well to spectroelectrochemical data for reduction of ZnNDI.[11a] Time-lapse UV-vis data shows a rapid initial reaction followed by a slower reduction process over several hours (Fig. S4†). After approximately 14 hours no further spectroscopic changes are observed. This is likely due to initial reduction of surface-exposed NDI ligands, followed by slower reduction of ligands throughout the framework, limited by diffusion of charge-balancing TBA^+ cations into the pores;[11c] consistent with this interpretation, the mesoporous MOF-74 analogue Ni-NDISA (33 Å pore diameter, compared to 16 Å for ZnNDI) undergoes complete reaction with TBAF in minutes rather than hours.‡[13] In contrast to data reported for NDI-based small molecules in solution,[12] we do not observe further reduction to the NDI^{2-} dianion form in ZnNDI upon longer soaking times or with increased amounts of fluoride, even though the ligand dianion is electrochemically accessible.[11a] The spectral features for the reduced MOF persist after removal from the TBAF solution if kept under an inert atmosphere, but rapidly decrease in intensity upon exposure to air (Fig. S5†). The spectrum of neutral ZnNDI is recovered after brief soaking in DMF that has not been deoxygenated (Fig. S6†).

Neutral, as-synthesized ZnNDI is an electrical insulator, with a conductivity value below the limit of detection for our instrumentation ($\leq 10^{-14}$ S cm^{-1}). To examine the effect of ligand reduction on conductivity, bulk samples were soaked in DMF solutions of TBAF for 24 hours. Different degrees of ligand reduction were achieved by soaking with varying amounts of fluoride (designated samples A–C; details given in the ESI†). Similar to the thin films, bulk powder samples of ZnNDI exhibited a color change from tan/yellow to black after reduction. After isolation by filtration, washing with fresh DMF and Et_2O, and vacuum drying, the reduced samples were characterized by PXRD to ensure that no structural changes or degradation occurred (Fig. 1b). Scanning electron microscopy also showed no significant changes in morphology after reduction (Fig. S7 and S8†). Reduced ZnNDI is stable for at least 1 month after isolation if kept under an inert atmosphere.

The extent of ligand reduction in ZnNDI was evaluated using quantitative EPR, with samples prepared as a 5% w/w mixture in an eicosane matrix. Quantitation of spins in this manner led to values of 7.5×10^{17} spins per mg for ZnNDI-A, 5.0×10^{17} spins per mg for ZnNDI-B, and 2.0×10^{17} spins per mg for ZnNDI-C. Calculating based on the general formula $[(TBA)_x(ZnNDI)]$, where one TBA^+ cation is incorporated per NDI ligand reduced to its radical anion form, the EPR data indicates the extent of ligand reduction to be approximately 90%, 50%, and 20% for samples A, B, and C, respectively (details of EPR data collection and analysis are given in the ESI†). The ability of NDI-based MOFs to accommodate high degrees of ligand reduction while maintaining structural stability is also supported by previous studies on electrochemical reduction.[11]

Room temperature conductivity values (pressed-pellet, 2-probe) for the reduced samples were measured, as shown in Fig. 3. Pellets of ZnNDI-A, with 90% of its ligands reduced to their radical anion form, displayed an average conductivity value of 2×10^{-7} S cm^{-1}, with a maximum observed value of 6×10^{-7} S cm^{-1}. All measured samples of ZnNDI-A displayed conductivity values at least 10^6 higher than the neutral material. Samples ZnNDI-B and ZnNDI-C, with lower degrees of ligand reduction, displayed average values of 1×10^{-9} and 3×10^{-10} S cm^{-1}, respectively, demonstrating that the doping level can be systematically varied in order to tune the conductivity of the material. While the maximum conductivity observed for ZnNDI-A does not approach record values for conductive MOFs, it is commensurate with other 3D MOFs featuring electroactive ligands and redox-inert metal centers. The most direct point of comparison is the well-studied family of porous tetrathiafulvalene (TTF)-based MOFs, which display average pressed-pellet conductivity values ranging from 10^{-9} to 10^{-6} S cm^{-1}.§[19]

To examine the stability of ZnNDI toward repeated redox cycling, the sample of ZnNDI-A displaying the highest

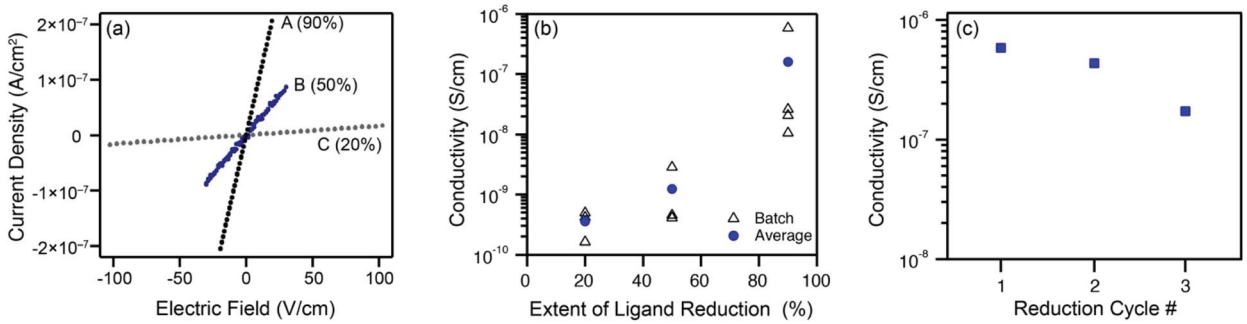

Fig. 3 Pressed-pellet conductivity measurements (2-probe, room temperature) on samples of ZnNDI after varying degrees of ligand reduction: (a) representative *I*–*V* curves, normalized for pellet size (extent of ligand reduction indicated in parenthesis); (b) conductivity values taken from multiple synthetic batches, showing systematic variations in conductivity as a function of ligand reduction; (c) conductivity of a single sample of ZnNDI-A that was subjected to three cycles of ligand reduction followed by aerobic re-oxidation. The neutral, as-synthesized MOF displays conductivity $\leq 10^{-14}$ S cm^{-1}.

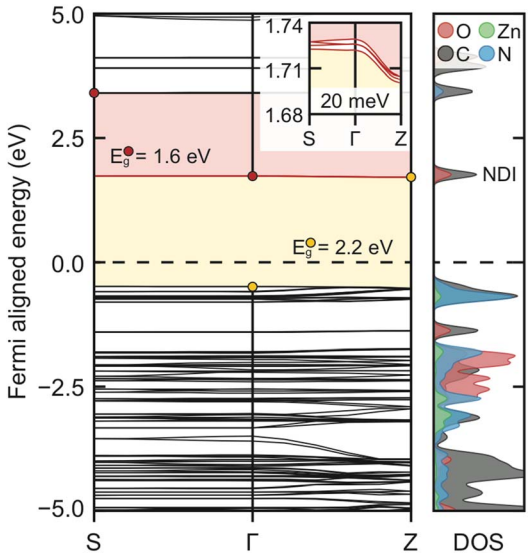

Fig. 4 Calculated electronic band structure and density of states for ZnNDI. In its neutral form, ZnNDI has a 2.2 eV band gap, which red-shifts to 1.6 eV upon population of the conduction band by ligand reduction.

conductivity value was subjected to three consecutive cycles of aerobic oxidation followed by fluoride-induced ligand reduction. Following each cycle of reduction and conductivity measurement, the sample was washed with aerated DMF under ambient atmosphere, followed by washing with acetone and vacuum drying. PXRD indicates that the structure remains unchanged after the reduced sample is air-exposed. As shown in Fig. 3c, only slight decreases in conductivity were observed over the course of three reduction cycles, with the overall order of magnitude of conductivity maintained.

Density functional theory calculations were used to further probe the electrical conductivity increase upon ligand reduction. The electronic band structure and projected density of states for the optimized ZnNDI structure are shown in Fig. 4, and detailed in the ESI.† The conduction band is defined by the NDI ligand orbitals, as clearly shown in orbital images of the DOS-labeled structure (Fig. S9a†). Curvature of the conduction band indicates electron mobility in that direction upon population *via* reductive doping (shown in the figure inset; *Z* corresponds to an out-of-plane 0, 0, 1/2 vector). Explicit calculation of ZnNDI with a single electron added to the system indicates spin delocalization over the NDI ligands (Fig. S9b†). Overall, these calculations support that electron conduction occurs *via* NDI hopping in the reduced ZnNDI materials. Furthermore, NDI reduction results in the emergence of super-gap excitations (Fig. 4, red), indicating a shift to a narrow gap material as the conduction band is populated; this is consistent with our experimental observation of new red-shifted bands in the UV-vis data.

Conclusions

We have reported the first example of electrical conductivity enhancement in a porous 3D MOF *via* ligand n-doping. The extent of ligand reduction in the redox-active MOF ZnNDI can be rationally varied, resulting in electrical conductivity values that span over six orders of magnitude. Notably, this work also represents the first demonstration of a 3D MOF that can be reversibly switched between two different stable redox states with dramatically different conductivities. Future work will aim to improve both switching times and maximum conductivity values.

Conflicts of interest

There are no conflicts to declare.

Acknowledgements

H. C. W., A. B. B., and M. G. C. thank the Department of Chemistry and the Office of the Provost at Barnard College for financial support. M. G. C. gratefully acknowledges the NSF (CHE-1827936) for a MRI award in support of a 400 MHz NMR spectrometer at Barnard College. PXRD was performed at the Shared Materials Characterization Laboratory at Columbia University. We thank Dr Amirali Zangiabadi for SEM imaging at the Columbia Nano Initiative electron microscopy facility. This work used the Extreme Science and Engineering Discovery Environment (XSEDE), which is supported by the National Science Foundation grant number ACI-1548562, and the PICS machine, Coeus, which is supported by the NSF (DMS1624776).

Notes and references

‡ Measurements of electrical conductivity for Ni-NDISA were unsuccessful due to framework collapse upon isolation and drying; see ref. 11*b* and 13.

§ Single crystal conductivity values up to 10^{-4} S cm^{-1} have been reported for TTF-based MOFs; it is well-established that pressed-pellet measurements underestimate intrinsic conductivity, especially when charge transport is expected to be anisotropic (see ref. 19*b* and *c*). We were unable to obtain material suitable for single crystal conductivity measurements of ZnNDI.

1 (*a*) L. Sun, M. G. Campbell and M. Dincă, *Angew. Chem., Int. Ed.*, 2016, **55**, 3566; (*b*) V. Stavila, A. A. Talin and M. D. Allendorf, *Chem. Soc. Rev.*, 2014, **43**, 5994; (*c*) M. D. Allendorf, A. Schwartzberg, B. Stavila and A. A. Talin, *Chem.–Eur. J.*, 2011, **17**, 11372.

2 (*a*) M. Hmadeh, Z. Lu, Z. Liu, F. Gándara, H. Furukawa, S. Wan, V. Augustyn, R. Chang, L. Liao, F. Zhou, E. Perre, V. Ozolins, K. Suenaga, X. Duan, B. Dunn, Y. Yamamoto, O. Terasaki and O. M. Yaghi, *Chem. Mater.*, 2012, **24**, 3511; (*b*) D. Sheberla, L. Sun, M. A. Blood-Forsythe, S. Er, C. R. Wade, C. K. Brozek, A. Aspuru-Guzik and M. Dincă, *J. Am. Chem. Soc.*, 2014, **136**, 8859; (*c*) X. Huang, P. Sheng, Z. Tu, F. Zhang, J. Wang, H. Geng, Y. Zou, C. Di, Y. Yi, Y. Sun and D. Zhu, *Nat. Commun.*, 2015, **6**, 7408; (*d*) A. J. Clough, N. M. Orchanian, J. M. Skelton, A. J. Neer, S. A. Howard, C. A. Downes, L. F. J. Piper, A. Walsh, B. C. Melot and S. C. Marinescu, *J. Am. Chem. Soc.*, 2019, **141**, 16323.

3 R. Murase, C. F. Leong and D. M. D'Alessandro, *Inorg. Chem.*, 2017, **56**, 14373.

4 (*a*) A. A. Talin, A. Centrone, A. C. Ford, M. E. Foster, V. Stavila, P. Haney, R. A. Kinney, V. Szalai, F. El Gabaly, H. P. Yoon, F. Léonard and M. D. Allendorf, *Science*, 2014, **343**, 66; (*b*) C.-W. Kung, K. Otake, C. T. Buru, S. Goswami, Y. Cui, J. T. Hupp, A. M. Spokoyny and O. K. Farha, *J. Am. Chem. Soc.*, 2018, **140**, 3871; (*c*) B. Le Ouay, M. Boudot, T. Kitao, T. Yanagida, S. Kitagawa and T. Uemura, *J. Am. Chem. Soc.*, 2016, **138**, 10088; (*d*) T. C. Wang, I. Hod, C. O. Audu, N. A. Vermeulen, S. T. Nguyen, O. K. Farha and J. T. Hupp, *ACS Appl. Mater. Interfaces*, 2017, **9**, 12584.

5 D. M. D'Alessandro, *Chem. Commun.*, 2016, **52**, 8957.

6 L. Sun, C. H. Hendon, S. S. Park, Y. Tulchinsky, R. Wan, F. Wang, A. Walsh and M. Dincă, *Chem. Sci.*, 2017, **8**, 4450.

7 M. L. Aubrey, B. M. Wiers, S. C. Andrews, T. Sakurai, S. E. Reyes-Lillo, S. M. Hamed, C.-J. Yu, L. E. Darago, J. A. Mason, J.-O. Baeg, F. Grandjean, G. J. Long, S. Seki, J. B. Neaton, P. Yang and J. R. Long, *Nat. Mater.*, 2018, **17**, 625.

8 L. S. Xie, L. Sun, R. Wan, S. S. Park, J. A. DeGayner, C. H. Hendon and M. Dincă, *J. Am. Chem. Soc.*, 2018, **140**, 7411.

9 (*a*) Y. Kobayashi, B. Jacobs, M. D. Allendorf and J. R. Long, *Chem. Mater.*, 2010, **22**, 4120; (*b*) L. E. Darago, M. L. Aubrey, C. J. Yu, M. I. Gonzalez and J. R. Long, *J. Am. Chem. Soc.*, 2015, **137**, 15703; (*c*) G. Skorupskii, B. A. Trump, T. W. Kasel, C. M. Brown, C. H. Hendon and M. Dincă, *Nat. Chem.*, 2019, DOI: 10.1038/s41557-019-0372-0.

10 (*a*) I.-R. Jeon, L. Sun, B. Negru, R. P. Van Duyne, M. Dincă and T. D. Harris, *J. Am. Chem. Soc.*, 2016, **138**, 6583; (*b*) L. Liu, J. A. DeGayner, L. Sun, D. Z. Zee and T. D. Harris, *Chem. Sci.*, 2019, **10**, 4652.

11 (*a*) C. R. Wade, M. Li and M. Dincă, *Angew. Chem., Int. Ed.*, 2013, **52**, 13377; (*b*) K. AlKaabi, C. R. Wade and M. Dincă, *Chem*, 2016, **1**, 264; (*c*) B. A. Johnson, A. Bhunia, H. Fei, S. M. Cohen and S. Ott, *J. Am. Chem. Soc.*, 2018, **140**, 2985.

12 S. Guha and S. Saha, *J. Am. Chem. Soc.*, 2010, **132**, 17674.

13 H. C. Wentz and M. G. Campbell, *Polyhedron*, 2018, **154**, 309.

14 (*a*) S. Saha, *Acc. Chem. Res.*, 2018, **51**, 2225; (*b*) G. Bélanger-Chabot, A. Ali and F. P. Gabbaï, *Angew. Chem., Int. Ed.*, 2017, **56**, 9958.

15 Q. Song, F. Li, Z. Wang and X. A. Zhang, *Chem. Sci.*, 2015, **6**, 3342.

16 C. J. Zhong, W. S. V. Kwan and L. L. Miller, *Chem. Mater.*, 1992, **4**, 1423.

17 C. R. Wade, T. Corrales-Sanchez, T. Narayan and M. Dincă, *Energy Environ. Sci.*, 2013, **6**, 2171.

18 G. Andric, J. F. Boas, A. M. Bond, G. D. Fallon, K. P. Ghiggino, C. F. Hogan, J. A. Hutchison, M. A.-P. Lee, M. S. J. Langford, J. R. Pilbrow, G. J. Troup and C. P. Woodward, *Aust. J. Chem.*, 2004, **57**, 1011.

19 (*a*) T. C. Narayan, T. Miyakai, S. Seki and M. Dincă, *J. Am. Chem. Soc.*, 2012, **134**, 12932; (*b*) S. S. Park, E. R. Hontz, L. Sun, C. H. Hendon, A. Walsh, T. Van Voorhis and M. Dincă, *J. Am. Chem. Soc.*, 2015, **137**, 1774; (*c*) L. Sun, S. S. Park, D. Sheberla and M. Dincă, *J. Am. Chem. Soc.*, 2016, **138**, 14772; (*d*) L. S. Xie and M. Dincă, *Isr. J. Chem.*, 2018, **58**, 1119; (*e*) L. S. Xie, E. V. Alexanderov, G. Skorupskii, D. Proserpio and M. Dincă, *Chem. Sci.*, 2019, **10**, 8558.